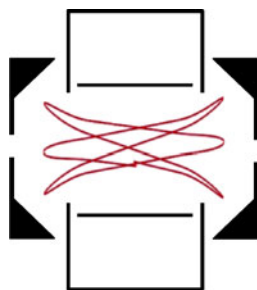


# Charge Detection Mass Spectrometry with Resolved Charge States

Nathan C. Contino, Elizabeth E. Pierson, David Z. Keifer, Martin F. Jarrold

Chemistry Department, Indiana University, 800 E. Kirkwood Avenue, Bloomington, IN 47405, USA



**Abstract.** Charge detection mass spectrometry (CDMS) measurements have been performed for cytochrome *c* and alcohol dehydrogenase (ADH) monomer using a modified cone trap incorporating a cryogenically cooled JFET. Cooling the JFET increases its transconductance and lowers thermal noise, improving the signal to noise (S/N) ratio. Single ions with as few as 9 elementary charges (*e*) have been detected. According to simulations, the detection efficiency for ions with a charge of 13 *e* is 75 %, and for charges above 13 *e* the detection efficiency rapidly approaches 95 %. With the low limit of detection achieved here, adjacent charge states are easily resolved in the *m/z* spectrum, so the accuracy and precision of the image charge measurements can be directly evaluated by

comparing the measured image charge to the charge deduced from the *m/z* spectrum. For ADH monomer ions with 32 to 43 charges, the root mean square deviation of the measured image charge is around 2.2 *e*. Ions were trapped for over 1500 cycles. The number of cycles detected appears to be limited mainly by collisions with the background gas.

**Key words:** Charge detection mass spectrometry

Received: 10 September 2012/Revised: 26 October 2012/Accepted: 29 October 2012/Published online: 30 November 2012

## Introduction

There has been growing interest in using mass spectrometry to investigate protein complexes [1–3] but their high masses present a challenge. Electrospray of proteins and protein complexes generate multiply-charged ions where the charge generally increases with the mass [4–6]. In conventional mass spectrometry, the *m/z* is measured for an ensemble of multiply-charged ions, and the charge is deduced from the separation between the peaks. The mass is then obtained from the charge and the *m/z*. This approach works well for multiply-charged ions with masses up to several hundred kilodalton but often breaks down for larger ions because the charge states are no longer resolved. Charge detection mass spectrometry (CDMS) can overcome this limitation [7–10]. In CDMS, the *m/z* and charge are directly measured for individual macro-ions, and then the mass is determined for each one. However, there have been challenges with implementing CDMS, in particular the poor accuracy of the charge measurement for an individual ion and the high limit of detection.

In CDMS, the charge is measured by passing the multiply-charged ion through a conducting cylinder and detecting the image charge with a charge-sensitive preamplifier. The main

limitation with this method is the low signal-to-noise ratio associated with directly measuring the small charge on a single macro-ion. It is not trivial to push the noise floor below 100 elementary charges (*e*). Both the accuracy and the limit of detection can be improved by signal averaging, using either a linear array of charge detectors [11–13] or a recirculating trap [14, 15] in which an ion is cycled back and forth through the same detector. Even with signal averaging, the limit of detection initially remained high, which prevented CDMS from fulfilling its promise as a useful analytical technique for the characterization of biological macromolecules and large, noncovalent assemblies. Recent work has focused on determining the charge and mass distributions for high molecular weight polymers [16, 17].

For CDMS to fully realize its potential, it is necessary to further reduce the uncertainty in the charge measurement and lower the limit of detection. Recently, we described a novel charge detection mass spectrometer where a dual hemispherical deflection analyzer (HDA) is coupled to a modified cone trap [18]. This apparatus offered longer trapping times than previously reported [14, 19], and the signals were analyzed using a method based on fast Fourier transforms (FFT). Ions with charges as small as 17 *e* were detected. However, the charge measurement was judged to be unreliable for ions with less than 30 charges. The uncertainty (rms deviation) in the measured charge for

charges greater than 30  $e$  was estimated from simulations to be approximately 3.2  $e$ .

In the work reported here we have once again significantly reduced the limit of detection and decreased the uncertainty in the charge measurement. This was accomplished by cryogenically cooling the JFET at the input of the charge sensitive preamplifier that senses the image charge. Cooling the JFET increases its transconductance and lowers thermal noise. With a cooled JFET, we were able to detect charge states as low as +9  $e$  for cytochrome  $c$ . With such a low limit of detection, it is easy to resolve adjacent charge states in the  $m/z$  spectrum. The resolution of charge states is significant because the measured image charge can be compared with the charge deduced from the  $m/z$  spectrum. This comparison allows direct experimental assessment of the accuracy and precision of the charge measurements.

## Experimental Methods

A detailed description of the apparatus has recently been provided [18], so only a brief description will be given here. Ions are generated by electrospray, desolvated by a counterflow of hot, dry air, and then passed into the vacuum chamber through a 0.5 mm diameter aperture. The ions enter the first differentially pumped region, which contains an ion funnel [20] with 96 plates. A DC gradient draws the ions towards the exit of the funnel while rf (around 600 kHz) from a home-built generator provides the pseudopotential that focuses the ions. After passing through the funnel, ions enter a differentially pumped region containing a hexapole ion guide, followed by another differentially pumped region containing a quadrupole. The ions are extracted from the quadrupole and focused using an asymmetric Einzel lens. The DC bias on the hexapole sets the nominal ion energy. In the work reported here, the DC bias was set to 100 V, so the nominal ion energy is 100 eV/ $z$ , where  $z$  is the number of elementary charges on the ion.

In the analysis region of the apparatus, the ions may be analyzed by an orthogonal reflectron time-of-flight mass spectrometer (TOF-MS) or by the charge detection mass spectrometer. The TOF-MS is used to characterize the electrospray source. To measure a TOF mass spectrum, the potentials on the Einzel lens are set to focus the ions into the extraction region of the TOF-MS. To measure a charge detection mass spectrum, the TOF extraction plates are grounded and the ion beam passes into the entrance of the dual hemispherical deflection analyzer. The dual HDA selects a narrow band of kinetic energies. In the studies reported here, the dual HDA was operated in a high resolution mode where the ions are decelerated to 10 % of their nominal kinetic energy for passage through the dual HDA. A retarding potential difference (RPD) energy analyzer was installed to measure the energy spread of the ion beam (which contains a distribution of charge states). The full width at half maximum (FWHM) is around 0.6 eV/ $z$  for ions with a nominal kinetic energy of 100 eV/ $z$ .

After passing through the dual HDA, the ions are focused into a modified cone trap [21]. The trap was designed to minimize the path length and maximize the trapping time. It consists of two conical end caps located at the ends of the charge detector tube. When an ion passes through the detector tube, an image charge of opposite sign is induced. The detector tube is connected to a JFET (2SK152) at the input of a charge-sensitive pre-amplifier (Amptek A250). Both the A250 and JFET are housed in the vacuum chamber, close to the detector. The signal from the A250 is passed outside of the vacuum chamber, where it is digitized with a home-built analog to digital converter and stored on a computer. Note that this detection scheme works equally well for ions with both positive and negative charges. To detect negative ions it is only necessary to reverse the polarity of the voltages.

With the voltages on the end caps of the cone trap set to +135 V, ions with nominal kinetic energies around 100 eV/ $z$  are trapped and cycle back and forth through the detector tube. At the start of a trapping cycle, the voltages on both the front and back cones are dropped from 135 V to ground and held there for 1 ms. During this time, ions enter and pass through the trap. The voltage on the back cone is raised to 135 V and then 12.5  $\mu$ s later the voltage on the front cone is raised. The front and back cones are maintained at the trapping voltage for around 29 ms, whereupon the voltages on the front and back end cap are dropped to ground to empty the trap and start the cycle again. The overall trapping efficiency (the fraction of ions trapped assuming they arrive at random intervals) is around 0.0005.

The periodic waveform that arises as the trapped ions pass back and forth through the charge detector tube is well-suited to analysis with a fast Fourier transform. The resulting frequency domain spectrum contains the fundamental frequency of the oscillatory motion and the associated harmonics. The relationship between the  $m/z$ , the fundamental frequency,  $f$ , and the nominal ion energy,  $E_o$ , was deduced empirically from SIMION simulations of ion trajectories in the trap. To a good approximation, the relationship is given by:

$$\frac{m}{z} = \frac{C}{E_o f^2} \quad (1)$$

where  $C$  is a constant that depends on the geometry of the cone trap and the applied voltages. The simulations also provide a value for the constant  $C$ . The dependence on the kinetic energy shown in Equation 1 is valid for trap geometries, kinetic energies, and voltages similar to those used here. A more complex dependence on kinetic energy may occur under different circumstances.

The magnitude of the fundamental frequency in the FFT is proportional to the image charge. The relationship between the magnitude and the charge was calibrated by applying a simulated signal with a known amplitude across a known capacitance into the gate of the JFET. This was done

with several different amplitudes and frequencies. The resulting signal was analyzed with a FORTRAN program to yield the charge calibration.

With the trapping scheme outlined above, more than one ion can be trapped at the same time. The signal is kept low to minimize the frequency of these multiple trapping events. In addition, the FORTRAN program that analyzes the experimental data rejects trapping events where more than one fundamental frequency is present in the Fourier transform. In the future, we hope to be able to analyze events where more than one ion is trapped but we have not yet developed the necessary algorithms. Two ions with the same charge and same kinetic energy that enter the trap at the same time and stay in phase will appear as a single ion with the correct  $m/z$  but with twice the charge. This series of coincidences does not occur very frequently.

The main difference between the apparatus employed here and that used previously<sup>18</sup> is that the JFET at the input of the charge sensitive preamplifier is cooled. This was accomplished by means of a liquid nitrogen reservoir connected to the JFET by a cold finger and copper braid. The temperature of the JFET was measured indirectly. Its temperature is estimated to be around 125 K. The temperature of the A250 and its external components are also lowered due to their proximity to the cooled JFET. Their temperatures were not measured, but it is likely that cooling these components contributes to the increased performance achieved here. Cooling improved the signal to noise ratio (S/N) by a factor of around 1.7.

All reagents were purchased from Sigma Aldrich. Cytochrome *c* (equine) was prepared at a concentration of 2 mg/mL in 1:1 water–methanol with 2 % vol/vol acetic acid. Alcohol dehydrogenase (*Saccharomyces cerevisiae*) was purified via size-exclusion chromatography and prepared at a concentration of 2 mg/mL in 1:1 water–methanol with 3 % vol/vol acetic acid. The active form of yeast alcohol dehydrogenase (ADH) is a tetramer; however, the tetramer breaks up into monomers at low pH [22].

## Results

As described above, the  $m/z$  for each ion is obtained from its oscillation frequency using Equation 1. The  $m/z$  values are then binned to generate a histogram. The upper half of Figure 1 shows an  $m/z$  histogram obtained for cytochrome *c* using a bin width of 5 Th. This histogram is the result of slightly less than 60,000 trapping events, each one lasting 30 ms (i.e., a total measurement time of 30 min). There are peaks in the histogram corresponding to charge states from +9 (at around 1350 Th) to +19 (at around 640 Th). A least squares fit to the peak centers in the  $m/z$  histogram yields a mass of 12,156 Da with an rms deviation in the  $m/z$  of 2.0 Th. The mass of equine cytochrome *c* is 12,386 Da [23], from which it appears that we underestimate the mass by around 1.9 %. The  $m/z$  resolution obtained from the width of the peaks in Figure 1 is approximately 0.015 full width at half maximum (FWHM). This is larger than anticipated on the

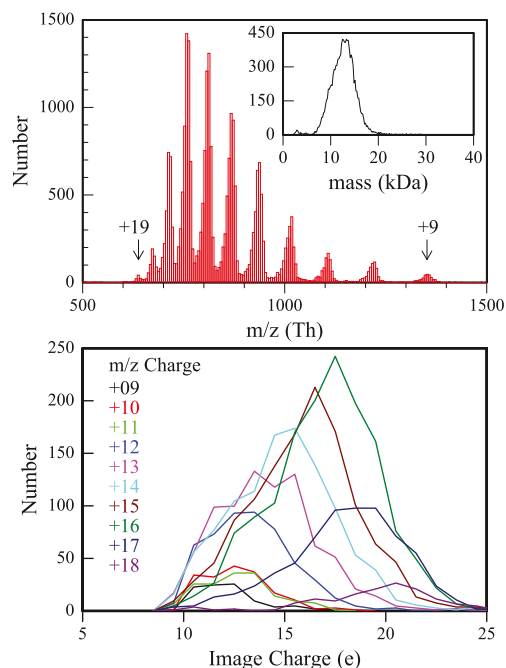


**Figure 1.** The upper plot shows an  $m/z$  histogram measured for cytochrome *c* by charge detection mass spectrometry. The inset shows the mass histogram obtained from the  $m/z$  and image charge for each ion. The lower plot shows image charge histograms for the +9 to +18 charge states of cytochrome *c*. The key on the left of this plot gives the color code to the  $m/z$  charge states

basis of the measured energy spread of the ions entering the trap which is around 0.006 (see above). One contribution to this discrepancy is that the oscillation frequency is slightly dependent on the ions' trajectory in the trap. SIMION simulations show that the trajectory in the trap depends on the entry conditions (both the angle and radial position). Ions that enter off-axis undergo trajectories reminiscent of Lissajous curves with oscillation frequencies that differ slightly from trajectories that oscillate along the axis of the trap. One cycle of such a trajectory is shown (not to scale) in the graphical abstract.

The mass of each ion can be obtained by multiplying its  $m/z$  by its measured image charge. The resulting masses can then be binned to obtain a mass histogram which is shown in the inset in the upper half of Figure 1. The mass histogram shows a single peak due to cytochrome *c*. There is no evidence for multimers. The average mass for the cytochrome *c* peak is 12,715 Da. This is larger than the expected mass because, as we discuss below, the image charge is overestimated by a few percent. The width of the mass distribution is mainly due to the inaccuracy of the image charge determination, which we quantify below.

The ions that contribute to the  $m/z$  histogram shown in the upper half of Figure 1 can be separated into their different charge states. For example, ions with  $m/z$  values between 735 and 775 Th correspond to the +16 charge state of cytochrome *c*. These +16 ions can be separated from the

other ions in the  $m/z$  histogram, and then the accuracy and precision of their image charge measurements can be examined. Histograms of the measured image charge for each  $m/z$  charge state are presented in the lower half of Figure 1. Results are shown for the +9 to +18 charge states (insufficient ions were found for the +19). Except for the low charge states, the center of the distributions systematically shift to higher charge as the  $m/z$  charge state increases. The distributions for the low charge states are substantially narrower than for the higher charge states.

The top half of Figure 2 shows the average image charge for the separated cytochrome  $c$  charge states plotted against the  $m/z$  charge. The solid line shows where the average image charge would fall if it corresponded exactly to the known  $m/z$  charge. The filled squares show the average image charge obtained from the data analysis program. The

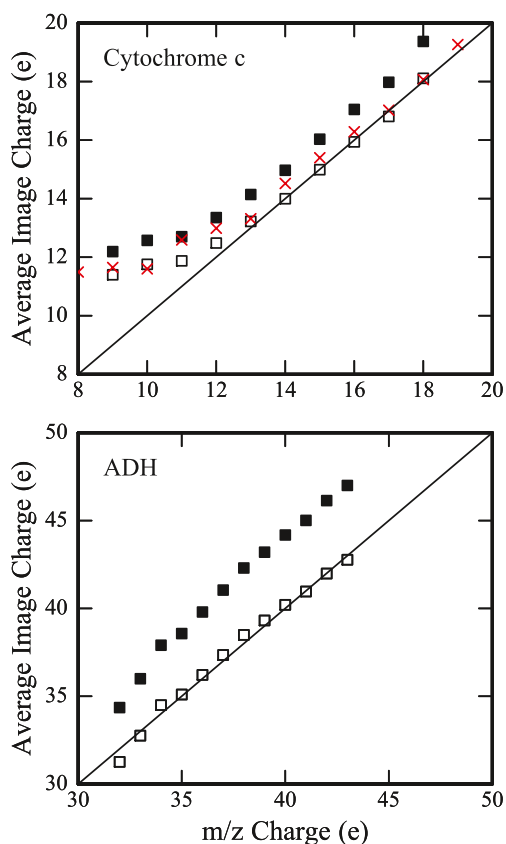


**Figure 2.** Plot of the average image charge against the  $m/z$  charge for cytochrome  $c$  (upper) and alcohol dehydrogenase monomer (lower). The solid line in both plots shows where the average image charge would fall if it corresponded exactly to the known  $m/z$  charge. The filled points show the results obtained directly from the data analysis program. The open points show the experimental results multiplied by a calibration factor that provides the best match to the known  $m/z$  charge. For cytochrome  $c$  the calibration factor is 0.935 and for alcohol dehydrogenase monomer it is 0.91. The red crosses in the upper plot show the average charge obtained from the cytochrome  $c$  simulations with the data analysis program (see text) plotted against the input charge

average image charge is systematically larger than the  $m/z$  charge. The open squares show the image charges multiplied by a calibration factor selected to provide the best match between the average image charges for the higher charge states and the known  $m/z$  charge. After this calibration factor is applied, the average image charges for the lower charges (<13 e) are still significantly larger than the  $m/z$  charge. The red crosses in the top half of Figure 2 are the result of simulations described below.

The standard deviation of the image charge distribution for each cytochrome  $c$  charge state is plotted on the left in Figure 3. The black circles show the experimental results and the red squares are the results of simulations described below. The standard deviation for the measured image charges increases from around 1.5 e for the +9 charge state to around 2.8 e for the +18 charge state.

Measurements similar to those described above were also performed for ADH monomer. Charge states from +30 to +46 were resolved in the  $m/z$  histogram. A least squares analysis of the peak positions yielded a mass of 35,506 which is 3.3 % smaller than the expected value of 36,718 Da [23]. A combined charge histogram for ADH monomer is shown in Figure 4. This histogram was obtained in the following way: first the average image charge was determined for the ions assigned to each charge state; then the relevant average was subtracted from the image charge for each ion; and finally the resulting charges were binned to give the combined histogram shown in the figure. The distribution is close to Gaussian. The red line in the figure is a Gaussian with a standard deviation of 2.17 e.

The average image charges for the ADH monomer are plotted against the  $m/z$  charge in the lower half of Figure 2. Again, the solid line shows where the average image charge

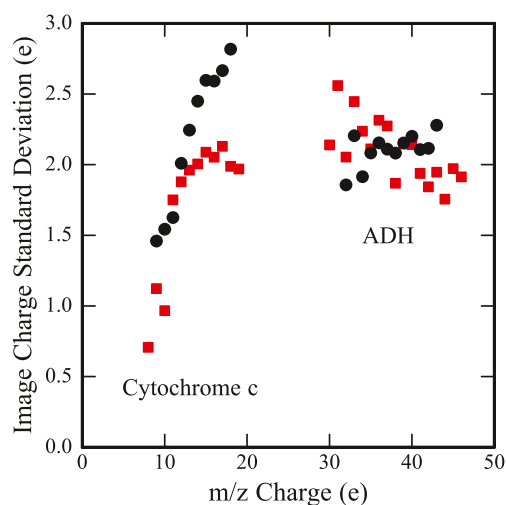


**Figure 3.** The standard deviation of the image charge distributions plotted against the  $m/z$  charge for cytochrome  $c$  (charges below 20 e) and alcohol dehydrogenase monomer (charges above 30 e). The black circles are the experimental results and the red squares are the result of simulations with the data analysis program (see text)

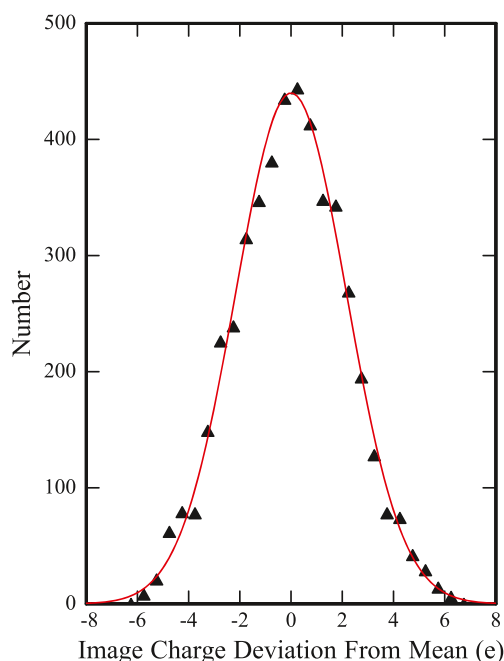


**Figure 4.** Combined image charge histogram for alcohol dehydrogenase monomer (see text). The points are the experimental results and the red line shows a Gaussian with a standard deviation of 2.17 e

would fall if it corresponded exactly to the known  $m/z$  charge. The filled squares show the average image charge obtained from the data analysis program. Results are shown for the +32 to +43 charge states. Outside this range, the number of ions per charge state was too small to obtain a reliable average. The average image charge is systematically larger than the  $m/z$  charge. The open squares show the image charges multiplied by a calibration factor selected to provide the best match between the average image charges and the known  $m/z$  charge.

The standard deviations of the image charge distributions for the individual ADH charge states are shown plotted against the  $m/z$  charge on the right hand side of Figure 3. The black circles are the experimental results and the red squares are the results of simulations described below. The experimental standard deviations for ADH are around 2 e, and appear to increase slightly with increasing  $m/z$  charge. The charge states for the ADH monomer are more closely spaced in the  $m/z$  histogram than those for cytochrome *c* and are not completely resolved. Thus there is the possibility of contamination where some ions from the  $n+1$  and  $n-1$  charge states are included with the  $n$  charge state ions. This will increase the standard deviation for the  $n$  charge state ions. Simulations were performed to determine the size of the error introduced by this charge contamination. The simulations indicate that it made a negligible contribution to the standard deviations for the ADH monomer.

The number of cycles detected for each ion is reported by the FORTRAN program used to analyze the data. Ions can be lost by physically leaving the trap or “lost” by the data

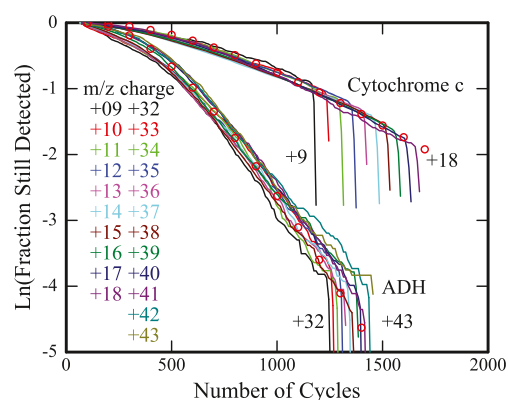


**Figure 5.** Plot of the natural log of the fraction of ions still detected against the number of cycles. Results are shown for cytochrome *c* (charge states from +9 to +18) and ADH monomer (charge states from +32 to +43). The charge states are color coded and the key is given in the figure. The red circles show the results of simulations based on multi-collision-induced loss (see text)

analysis program. Figure 5 shows a plot of the natural log of the fraction of ions still detected as a function of the number of cycles. Results are shown for the +9 to +18 charge states of cytochrome *c* and the +32 to +43 charge states of the ADH monomer. The vertical lines at the end of each data set result from ions that are detected to the end of the 29 ms trapping period. For a constant mass, ions with more charge have a smaller  $m/z$  and a larger velocity and, hence, the maximum number of cycles experienced during the trapping period is larger. The lines for the different charge states in Figure 5 are color coded, and the key is given on the left in the figure. The higher charge states of cytochrome *c* are trapped for more than 1500 cycles.

A plot of the natural log of the fraction of ions still detected against the number of cycles (as shown in Figure 5) should be linear if this fraction shows a first order decay. The plots are clearly not linear at the beginning of the trapping time but become more linear at longer trapping times. In the region where the plots are close to linear, the ADH ions decay around 2.5 times faster than the cytochrome *c* ions.

## Discussion

The masses of both cytochrome *c* and ADH monomer determined from the  $m/z$  distributions are underestimated by a few percent. The main source of uncertainty in the measured  $m/z$  values is in the constant  $C$  in Equation 1 that calibrates the relationship between the fundamental frequency at a given kinetic energy and the  $m/z$ . The constant  $C$  is obtained from SIMION simulations. The value of  $C$  used here apparently underestimates the mass by 2 %–3 %.

It is evident from Figure 2 that the average image charges from the data analysis program (filled points) are significantly larger than the  $m/z$  charges for both cytochrome *c* and

ADH monomer. This discrepancy is probably mainly due to the fact that the image charge measurements were calibrated at room temperature, whereas the measurements themselves were performed with the JFET cooled to around 125 K. Calibration at 125 K must be performed under vacuum, and we were not able to calibrate under vacuum during the course of these measurements. In addition, the calibration is performed with thousands of elementary charges, and it is unlikely that the response of the electronics will remain perfectly linear from the high charges used to calibrate to the small charges detected here. Because we are able to detect such small charges and because we have resolved the  $m/z$  charge states, we are able to calibrate the charges at much lower values than before.

Simulations were performed to further examine the performance of the modified cone trap with the cooled JFET. First, noise files were recorded by applying all voltages to the experiment but without introducing any ions into the vacuum chamber. Then simulated signals were added to the noise files. To make the simulations realistic, each simulated ion was given a random trapping time. The simulated signals were then analyzed by the FORTRAN program used to analyze the experimental data. We analyzed 200 ions for each charge state for cytochrome *c* and ADH monomer.

If the signal becomes too small, it will be overwhelmed by the noise and not detected by the data analysis program. Figure 6 shows the fraction of the simulations that were detected by the program plotted against the input charge. The results with input charges less than 20 e were obtained from the cytochrome *c* simulations and those for input charges greater than 30 e were obtained from ADH monomer simulations. The fraction detected remains high (>90 %) down to charges as small as 16 e. Below 16 e the

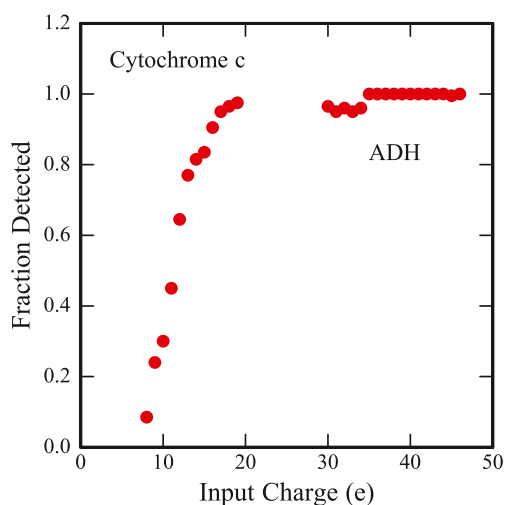


**Figure 6.** The fraction of signals that were detected in simulations with the data analysis program (see text) plotted against the input charge. The results with input charges less than 20 e were obtained with cytochrome *c* and those with input charges greater than 30 e were obtained with ADH monomer

fraction detected falls rapidly, dropping to around 25 % at 9 e. In the simulations, cytochrome *c* ions with as few as eight charges were detected, albeit with a low probability (8.5 %). The smallest charge detected in the experiments is +9, possibly because the abundance of the cytochrome *c* +8 charge state is low under the conditions used here.

The red crosses in Figure 2 show the average charge obtained from the simulations for cytochrome *c* plotted against the input charge. The solid line shows where the average charge should be if it were in perfect agreement with the input charge. For charges of 13 e and greater, there is good agreement between the input charge and the average charge deduced from the simulation. For charges less than 13 e, the average charge from the simulation diverges from the input charge. This divergence is also seen in the experimental data (see Figure 2). It is believed to result from increased detection efficiency for ions where the noise enhances the signal and decreased detection efficiency where the noise diminishes the signal. When the charge is close to the limit of detection, the detection efficiency increases when the signal is enhanced by noise and decreases when it is diminished, so the average measured charge is skewed to falsely high charge. For a larger charge, both noise-enhanced and noise-diminished signals are detected with the same probability, and so the average measured charge more closely approximates the input charge. The same effect is responsible for the narrowing of the image charge distribution that occurs for the lower charge states of cytochrome *c* (see Figure 1).

The skewing of the average measured image charge mentioned above only becomes important for ions with less than 13 charges in both the experimental data and in the simulations (Figure 2), so 13 e is the smallest charge that can be accurately measured with the present experimental configuration. According to Figure 6, greater than 75 % of the 13 e ions were detected by the data analysis program in the simulations.

Standard deviations for the charge distributions obtained from the simulations are plotted in Figure 3 as red squares. The standard deviations for ADH monomer simulations are close to the measured values: both average around 2.1 e, although in the experimental data the standard deviations appear to increase slightly with increasing charge, whereas for the simulations it appears that this trend is reversed. The standard deviations for the cytochrome *c* simulations with input charges >13 e have values around 2.0 e; however, for smaller input charges, the standard deviations decrease sharply with decreasing charge. The skewing of the image charge distributions mentioned above is responsible for this decrease.

For charges <13 e, the standard deviations for the measured data behave in a similar way to those for the simulations—they both increase with increasing charge (see Figure 2). However, for charges above 13 e, the standard deviation for the simulations level off at around 2.0 e, whereas those for the measured data continue to increase, eventually reaching around 2.8 e. Inspection of the individual image charge distributions shown in the lower half of Figure 1 reveal the cause of this difference. The image charge

distributions for the higher charge states show a tail that extends to low charge. The fact that a tail is not observed in the simulations leads us to believe that it is not an artifact of the data analysis program. One possible explanation is that there is an impurity with roughly the same  $m/z$  as the higher cytochrome *c* charge states, but with lower charges. There is not clear evidence for such an impurity in the TOF  $m/z$  spectrum. However, the purported impurity is present in low abundance and may not display well-resolved  $m/z$  peaks. There is a broad low intensity background in the TOF  $m/z$  spectrum, so we cannot rule out this explanation.

Zajfman and collaborators [24–26] have reported several studies using an ion trap related to the one used here. They were interested in trapping ensembles of atomic ions or small molecular ions. They reported that the lifetime of the ions in their trap was determined by collisions with the background gas. If a single collision were enough to cause the ions to be lost, the plots in Figure 5 would be linear. They are clearly not linear. However, the nonlinearity could be explained by a loss process where multiple collisions are required for ions to be lost.

Both cytochrome *c* and ADH were electrosprayed from acidified solutions. For cytochrome *c*, cross sections from ion mobility measurements indicate an unfolded geometry in the gas phase [27, 28]. The ADH monomer is also expected to have an unfolded geometry with the conditions employed. For unfolded geometries, the collision cross sections are expected to roughly scale linearly with the mass of the protein. The mass of the ADH monomer is approximately three times larger than the mass of cytochrome *c*, and so the cross sections for ADH should be around three times larger than the cross sections for cytochrome *c*. As described above, the slopes of the lines in the linear portions of the plots indicate that the ADH monomer ions are lost around 2.5 times more quickly than the cytochrome *c* ions.

Simulations were performed to test the idea that the results in Figure 5 could be explained by a loss process involving multiple collisions. We define a probability ( $\lambda$ ) that the ion experiences a collision during a single trapping cycle and then use a Poisson distribution to calculate the probability that the ions experiences  $j$  collisions after undergoing  $m$  cycles:

$$P(j, m, \lambda) = \frac{(m\lambda)^j e^{-m\lambda}}{j!} \quad (2)$$

We then define  $j_{loss}$  as the number of collisions required to lose an ion. The fraction of ions that are still detected as a function of the number of cycles is then given by:

$$F_{trapped}(j, m, \lambda) = \sum_{j=0}^{j_{loss}-1} \frac{(m\lambda)^j e^{-m\lambda}}{j!} \quad (3)$$

There are two adjustable parameters in this model: the collision probability per cycle ( $\lambda$ ) and the number of

collisions required for an ion to be lost ( $j_{loss}$ ). We adjusted these parameters manually to obtain a good fit to experimental data. The results are plotted in Figure 5 as the red circles. A good fit to the ADH monomer data was obtained with  $j_{loss}=4$  and  $\lambda=0.0072$  and a good fit to the cytochrome *c* data was achieved with  $j_{loss}=3$  and  $\lambda=0.0028$ . The ratio of the collision probabilities obtained from the fits is close to the expected ratio of the ion mobility collision cross sections. The absolute values of the collision probabilities are within 20 % of the values calculated from the ion mobility collision cross sections and the background pressure in the chamber, as measured by an ion gauge. These results suggest that the main factor causing ions to be lost is collisions with the background gas.

There is another factor that should be mentioned, which is the energy expended in charging the gate capacitance of the FET every time an ion enters the charge detection cylinder. This energy comes from the ion's kinetic energy, so the ion will decelerate and eventually it will be lost from the trap. The energy lost per cycle can be estimated from  $(ze)^2/(2C_{eff})$  where  $C_{eff}$  is the effective gate capacitance. In this work, the energy lost through this mechanism is very small, and it can be safely neglected.

The accuracy of the image charge measurements reported here is the best that has been achieved so far. The rms deviation ( $\sigma$ ) is around 2.2 e. To be able to assign the charge state with a high degree of confidence (99.7 %), it is necessary to measure the image charge with an accuracy given by  $3\sigma \leq 0.5$  e or  $\sigma \leq 0.1667$  e. We are still at least an order of magnitude away from achieving this goal. The S/N ratio limits the accuracy of the image charge measurement. It should be possible to lower the noise further, but it is doubtful that a gain of more than a factor of 2 can be realized without a paradigm shift.

A reviewer suggested that having more than one detector in the trap might provide an improvement in the accuracy of the charge measurement. The first trap we built incorporated an array of four detectors. It was not very successful. We switched to the one detector trap used here and we were able to trap the ions for much longer. A short one-detector trap appears to be more forgiving than a long multidetector trap. A better designed multidetector trap may change this situation, but the improvement over the one detector trap will probably not be large.

Some additional improvement in the accuracy of the charge determination may be realized by modifying and fine-tuning the method used to analyze the data. The only other option is to increase the signal length. The S/N ratio should scale with the square root of the signal length, so it is necessary to lengthen the signal by a factor of  $10^2$  to obtain an order of magnitude improvement in the S/N ratio. From the results presented above, the length of the signal is limited by the background pressure, so the required accuracy can be achieved by lowering the pressure by two orders of magnitude.

## Conclusions

Cryogenically cooling the input FET improves the S/N by a factor of around 1.7. With this improvement, the image charge can be measured for ions with a charge of 9 e. With the low limit of detection achieved here it is easy to resolve neighboring charge states in the  $m/z$  spectrum so that the image charge can be compared with the charge deduced from the  $m/z$  spectrum. The rms deviation of the measured image charge from the  $m/z$  charge is around 2.2 e for the +32 to +43 charge states of ADH monomer.

## Acknowledgments

The authors gratefully acknowledge the support of the National Science Foundation through award number 0832651. This work was partially supported by a grant from the METACyt Initiative, Indiana University. The authors are grateful for the technical assistance of Mr. Andy Alexander and Mr. John Poehlman in Electronic Instrument Services and Mr. Delbert Allgood in Mechanical Instrument Services.

## References

- Kaddis, C.S., Lomeli, S.H., Yin, S., Berhane, B., Apostol, M.I., Kickhoefer, V.A., Rome, L.H., Loo, J.A.: Sizing large proteins and protein complexes by electrospray ionization mass spectrometry and ion mobility. *J. Am. Soc. Mass Spectrom.* **18**, 1206–1216 (2007)
- Heck, A.J.R.: Native mass spectrometry: A bridge between interactomics and structural biology. *Nature Methods* **5**, 927–933 (2008)
- Freeke, J., Bush, M.F., Robinson, C.V., Ruotolo, B.T.: Gas-phase protein assemblies: Unfolding landscapes and preserving native-like structures using noncovalent adducts. *Chem. Phys. Letts.* **524**, 1–9 (2012)
- Fenn, J.B., Mann, M., Meng, C.K., Wong, S.F., Whitehouse, C.M.: Electrospray ionization for mass spectrometry of large biomolecules. *Science* **246**, 64–71 (1989)
- Loo, J.A., Udseth, H.R., Smith, R.D.: Peptide and protein analysis by electrospray ionization mass spectrometry and capillary electrophoresis-mass spectrometry. *Anal. Biochem.* **179**, 404–412 (1989)
- de la Mora, J.F.: Electrospray ionization of large multiply charged species proceeds via dole's charge residue mechanism. *Anal. Chim. Acta* **406**, 93–104 (2000)
- Fuerstenau, S.D., Benner, W.H.: Molecular weight determination of megadalton DNA electrospray ions using charge detection time-of-flight mass spectrometry. *Rapid Commun. Mass Spectrom.* **9**, 1528–1538 (1995)
- Schultz, J.C., Hack, C.A., Benner, W.H.: Mass determination of megadalton-dna electrospray ions using charge detection mass spectrometry. *J. Am. Soc. Mass Spectrom.* **9**, 305–313 (1998)
- Schultz, J.C., Hack, C.A., Benner, W.H.: Polymerase chain reaction products analyzed by charge detection mass spectrometry. *Rapid Commun. Mass Spectrom.* **13**, 15–20 (1999)
- Fuerstenau, S.D., Benner, W.H., Thomas, J.J., Brugidou, C., Bothner, B., Siuzdak, G.: Mass spectrometry of an intact virus. *Angew. Chem. Int. Ed.* **40**, 541–544 (2001)
- Gamero-Castano, M.: Induction charge detector with multiple sensing stages. *Rev. Sci. Instrum.* **78**, 043902 (2007)
- Gamero-Castano, M.: Retarding potential and induction charge detectors in tandem for measuring the charge and mass of nanodroplets. *Rev. Sci. Instrum.* **80**, 053301 (2009)
- Smith, J.W., Siegel, E.E., Maze, J.T., Jarrold, M.F.: Image charge detection mass spectrometry: pushing the envelope with sensitivity and accuracy. *Anal. Chem.* **83**, 950–956 (2011)
- Benner, W.H.: A Gated electrostatic ion trap to repetitiously measure the charge and  $m/z$  of large electrospray ions. *Anal. Chem.* **69**, 4162–4168 (1997)
- Sun, Q., Ding, L., Gu, C.: Modeling and optimization of dual-cylinder image current detector in electrostatic ion beam trap for mass spectrometry. *Int. J. Mass Spectrom.* **282**, 38–44 (2009)
- Doussineau, T., Kerleroux, M., Dagany, X., Clavier, C., Barbaire, M., Maurelli, J., Antoine, R., Dugourd, P.: Charging megadalton poly(ethylene oxide)s by electrospray ionization. A charge detection mass spectrometry study. *Rapid Commun. Mass Spectrom.* **25**, 617–623 (2011)
- Doussineau, T., Bao, C.Y., Antoine, R., Dugourd, P., Zhang, W., D'Agosto, F., Charleux, B.: Direct molar mass determination of self-assembled amphiphilic block copolymer nanoobjects using electrospray-charge detection mass spectrometry. *ACS Macro Lett.* **1**, 414–417 (2012)
- Contino, N.C., Jarrold, M.F.: Charge detection mass spectrometry for single ions with a limit of detection of 30 charges. *Int. J. Mass Spectrom.* (2012). doi:10.1016/j.ijms.2012.07.010
- Doussineau, T., Bao, C.Y., Clavier, C., Dagany, X., Kerleroux, M., Antoine, R., Dugourd, P.: Infrared multiphoton dissociation tandem charge detection-mass spectrometry of single megadalton electrosprayed ions. *Rev. Sci. Instrum.* **82**, 084104 (2011)
- Kelly, R.T., Tolmachev, A.V., Page, J.S., Tang, K., Smith, R.D.: The ion funnel: Theory, implementation, and applications. *Mass Spectrom. Rev.* **29**, 294–312 (2010)
- Schmidt, H.T., Cederquist, H., Jensen, J., Fardi, A.: Conetrap: A compact electrostatic ion trap. *Nucl. Instrum. Methods B* **173**, 523–527 (2001)
- Loo, J.A.: Observation of large subunit protein complexes by electrospray ionization mass spectrometry. *J. Mass Spectrom.* **30**, 180–183 (1995)
- Sequence mass from [www.uniprot.org](http://www.uniprot.org). For cytochrome *c* we add the mass of heme *c*.
- Dahan, M., Fishman, R., Heber, O., Rappaport, M., Altstein, N., Zajfman, D., van der Zande, W.J.: A new type of electrostatic ion trap for storage of fast ion beams. *Rev. Sci. Instrum.* **69**, 76–83 (1998)
- Wolf, A., Bhushan, K.G., Ben-Itzhak, I., Altstein, N., Zajfman, D., Heber, O., Rappaport, M.L.: Lifetime measurement of  $he^+$  using an electrostatic ion trap. *Phys. Rev. A* **59**, 267–270 (1999)
- Zajfman, D., Rudich, Y., Sagi, I., Strasser, D., Savin, D.W., Goldberg, S., Rappaport, M., Heber, O.: High resolution mass spectrometry using a linear electrostatic ion beam trap. *Int. J. Mass Spectrom.* **229**, 55–60 (2003)
- Clemmer, D.E., Hudgins, R.R., Jarrold, M.F.: Naked protein conformations: Cytochrome *c* in the gas phase. *J. Am. Chem. Soc.* **117**, 10141–10142 (1995)
- Shelimov, K.B., Clemmer, D.E., Jarrold, M.F.: Protein structure in vacuo: The gas phase conformations of BPTI and cytochrome *c*. *J. Am. Chem. Soc.* **119**, 2240–2248 (1997)